NUMERICAL SIMULATION STUDY ON THE MICRO FLOW LAW OF SUPERCRITICAL CO_2 IN POROUS MEDIA OF RESERVOIRS

by

Ping XIE[a,b], Mengmeng ZHOU[a,b], Haizhu WANG[a,b*], Bin WANG[a,b], Runzi XU[b], and Zhuoxin DONG[b]

[a] State Key Laboratory of Petroleum Resources and Engineering, China University of Petroleum, Beijing, China
[b] College of Petroleum Engineering, China University of Petroleum, Beijing, China

Original scientific paper
https://doi.org/10.2298/TSCI2404529X

Through the development of a mathematical model for micro-scale multi-phase flow of supercritical CO_2 and a simplified geological reservoir micro-model, numerical simulations were executed using the open-source CFD software Open FOAM. The study systematically analyzed various engineering and geological parameters' influence on the micro-scale flow patterns of supercritical CO_2 under reservoir temperature and pressure conditions. These insights provide guidance for designing process parameters in fracturing and storing supercritical CO_2.

Key words: *supercritical CO_2, micromodel, two-phase flow, numerical simulation*

Introduction

Carbon capture and storage (CCS) is employed to effectively sequester CO_2 underground [1], thereby reducing its atmospheric emissions. Carbon capture, utilization, and storage (CCUS) technology, building upon CO_2 storage, goes a step further by utilizing captured CO_2 [2, 3]. The CCUS encompasses the capture of CO_2 and its related compounds from production sources, the compression, transportation, and utilization of the captured CO_2, including processes like injection into deep geological formations for permanent storage and injection into existing oil fields to enhance oil recovery [4].

Currently, research on CCUS primarily focuses on CO_2 storage site selection, the quantity of CO_2 storage, and storage safety studies. Zhao, *et al.* [5], under conditions of 277.15 K and 3.0 MPa, utilized magnetic resonance imaging (MRI) technology to dynamically monitor the distribution of formation water. Kolawole, *et al.* [6] conducted geological mechanical tests on deep-seated carbonate rock samples before and after treatment with microbial culture medium and supercritical CO_2 ($ScCO_2$), using SEM and X-ray Diffraction (XRD). They assessed the mechanical, chemical, and microscopic structural responses of carbonate rocks exposed to $ScCO_2$, considering the presence or absence of microbial media in the pore volume.

In this study, we established a simplified micro-model for CO_2 geological storage formations. Utilizing the open-source computational fluid dynamics software Open FOAM [7], we conducted numerical simulations, analyzed the influence of various engineering and geological parameters like CO_2 injection speed, reservoir temperature and wettability, on the mi-

* Corresponding author, e-mail: whz0001@126.com

croscopic flow patterns during CO_2 geological storage under reservoir temperature and pressure conditions.

The establishment and validation of the microscopic model

The governing equations

In the microscopic model, the physical process of two-phase displacement can be described by the Navier-Stokes equations, specifically the fluid momentum conservation equation. Consequently, we can obtain [8, 9]:

$$\frac{\partial(\rho\vec{\mathrm{v}})}{\partial t}+\nabla(\rho\vec{\mathrm{v}}\vec{\mathrm{v}})+\nabla p-\nabla\left[\mu\left(\nabla\vec{\mathrm{v}}+\nabla^{T}\vec{\mathrm{v}}+\vec{f}\right)\right]=0,\ \vec{\mathrm{f}}=\sigma k\vec{\mathrm{n}}\delta_{\Gamma_\tau} \tag{1}$$

where ρ is the fluid density, $\vec{\mathrm{v}}$ – the fluid velocity, p – the fluid pressure, μ – the fluid viscosity, $\vec{\mathrm{f}}$ – the contribution of capillary forces at the fluid-fluid interface to momentum, σ – the interfacial tension between the two-phases, k – the interface curvature, $\vec{\mathrm{n}}$ – the unit normal vector pointing towards the wetting phase at the interface, and δ_{Γ_τ} – the Dirac delta function.

We now consider the fluid volume fraction α to characterize the spatial location of the fluid-fluid interface:

$$\alpha=\begin{cases}0, & \text{nonwetting phase}\\ 1, & \text{wetting phase}\\ 0\sim 1, & \text{interface}\end{cases} \tag{2}$$

In the fluid volume method, the evolution of the volume fraction can be described by [10]:

$$\frac{\partial\alpha}{\partial t}+\nabla(\alpha\vec{\mathrm{v}})+\nabla\left[\alpha(1-\alpha)\vec{\mathrm{v}}_r\right]=0 \tag{3}$$

where $\vec{\mathrm{v}}_r$ is the artificially constructed velocity to enhance the stability of the algorithm at the interface.

Based on eq. (2), it can be inferred that the density and viscosity of the fluid in eq. (1) can be expressed as functions of volume fraction. Here:

$$\rho(\alpha)=\alpha\rho_o+(1-\alpha)\rho_{\mathrm{CO}_2} \tag{4}$$

$$\mu(\alpha)=\alpha\mu_o+(1-\alpha)\mu_{\mathrm{CO}_2} \tag{5}$$

where ρ_o and ρ_{CO_2} [kgm^{-3}] are the density of oil and CO_2, while ρ_o and ρ_{CO_2} [Pa·s] – the viscosity of oil and CO_2.

Taking into account the interface normal vector $\vec{\mathrm{n}}=\nabla\alpha$ and $\nabla\vec{\mathrm{v}}=0$, we obtain the governing equations for the motion of CO_2 and oil in two-phase flow [11]:

$$\begin{gathered}\frac{\partial\left[\rho(\alpha)\vec{\mathrm{v}}\right]}{\partial t}-\nabla\left[\mu(\alpha)\left(\nabla\vec{\mathrm{v}}+\nabla^{T}\vec{\mathrm{v}}\right)+\nabla\rho(\alpha)\vec{\mathrm{v}}\vec{\mathrm{v}}\right]+\nabla p+\sigma\nabla\left(\frac{\nabla\alpha}{\nabla\alpha}\right)\nabla\alpha\delta_\Gamma=0\\ \nabla\vec{\mathrm{v}}=0\\ \frac{\partial\alpha}{\partial t}+\nabla(\alpha\vec{\mathrm{v}})+\nabla\left[\alpha(1-\alpha)\vec{\mathrm{v}}_r\right]=0\end{gathered} \tag{6}$$

where σ is the interfacial tension between the two-phases.

In fact, the scaling-law models for the Navier-Stokes-type equations were considered to the scaling-law flows [12, 13], which are the generalized versions of the Navier-Stokes equations.

Model establishment

Simplifying assumptions

To simplify calculations, we utilize the maximum inscribed circle method to organize pores and throats, establishing a geometric model with randomly distributed micro-pillars. The following assumptions are made regarding the established pore structure model: All reservoir matrix is assumed to be cylindrical. The coupling between the reservoir matrix and reservoir fluid is neglected. The height of matrix micro-pillars is uniform, *i.e.*, the depths of all parts of the model are the same. Nanoscale pores and throats with negligible convective contributions are ignored. All pore sizes are at the micron scale. Based on the aforementioned assumptions, we employed CAD drawing and Python programming to generate a random distribution of micro-pillars. The parameters for the pores, tab. 1.

Table 1. Microscopic model pore structure parameters

Number of micro-pillars	Matrix micro-pillar diameter [μm]	Throat depth [μm]	Throat width [μm]		
			Minimum	Maximum	Average
10473	10~80	4.5	10	110	56

Simulation results of fluid distribution

Here we kept the reservoir pressure at 12 MPa, the wet angle at 45°, and the constant injection rate at 0.0005 m/s, and studied the two-phase flow rules of CO_2 under different formation temperatures (35 °C, 40 °C, 45 °C, 50 °C, and 55 °C). As shown in figs. 1 and 2, the migration of supercritical CO_2 fluid is significantly influenced by reservoir temperature. As the

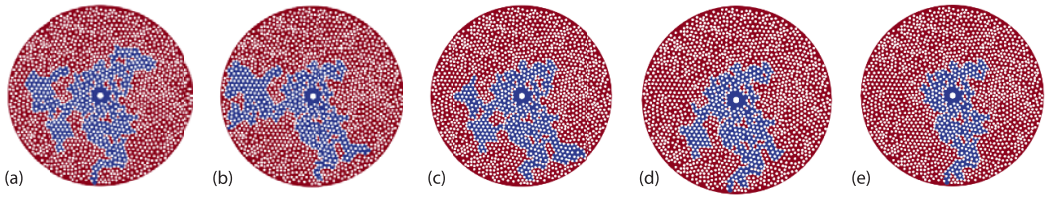

Figure 1. Influence of reservoir temperature on the distribution of Sc-CO_2 fluid; (a) T = 35 °C, (b) T = 40 °C, (c) T = 45 °C, (d) T = 50 °C, and (e) T = 55 °C

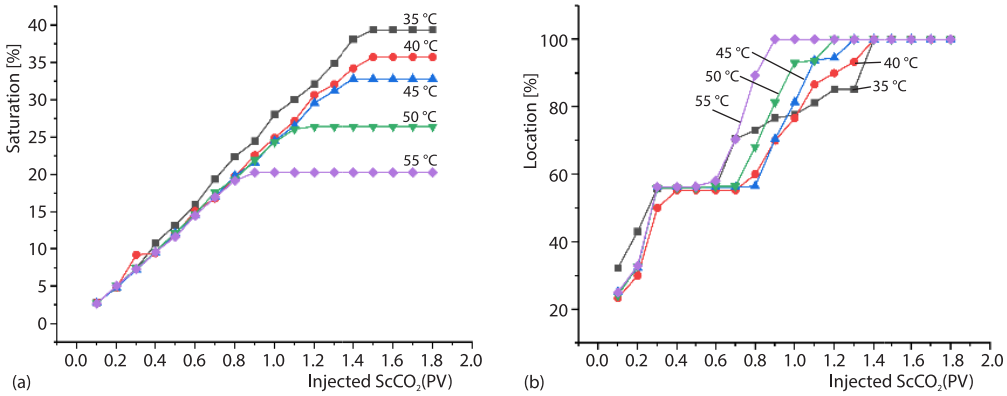

Figure 2. Influence of temperature on the transport of Sc-CO_2; (a) proportion of Sc-CO_2 saturation and (b) normalized displacement front distance

reservoir temperature increases, the time for CO_2 front movement to reach the model boundary rapidly shortens, indicating an accelerated movement of CO_2 with higher reservoir temperatures. Simultaneously, the proportion of CO_2 saturation decreases. This suggests that under high temperature conditions, CO_2 is more prone to diffusion, facilitating faster CO_2 sequestration. However, the ability of CO_2 to fill the pore space of the reservoir model weakens, favoring expansion along a single preferential channel in the forward direction.

Reservoir wettability

Reservoir wettability has a relatively significant impact on fluid migration patterns, as shown in figs. 3(a)-3(e). With an increase in wettability angle, transitioning from oil-wet to water-wet conditions, the dominant channels gradually diminish, and the finger invasion phenomenon weakens. The influence of reservoir porosity on fluid distribution diminishes. When the wettability angle increases, as shown in fig. 4(a), the percentage of the total pore volume occupied by CO_2 increases when it reaches the model boundary. From fig. 4(b), we can see that the time for the CO_2 front to stop moving forward shortens. When the wettability angle is greater than 90°, there is no longer a noticeable stagnation in CO_2 migration. The arrival time of the fluid front at the reservoir model boundary extends. Thus, transitioning from oil-wet to water-wet conditions enhances the efficiency of Sc-CO_2 penetration, making storage smoother and more thorough.

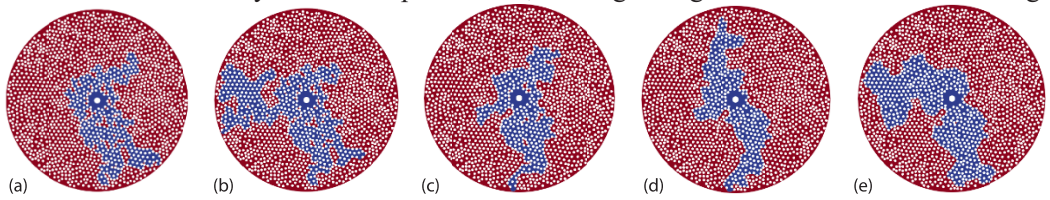

Figure 3. Influence of reservoir wettability on Sc-CO_2 fluid distribution; (a) θ = 10°, (b) θ = 45°, (c) θ = 90°, (d) θ = 135°, and (e) θ = 150°

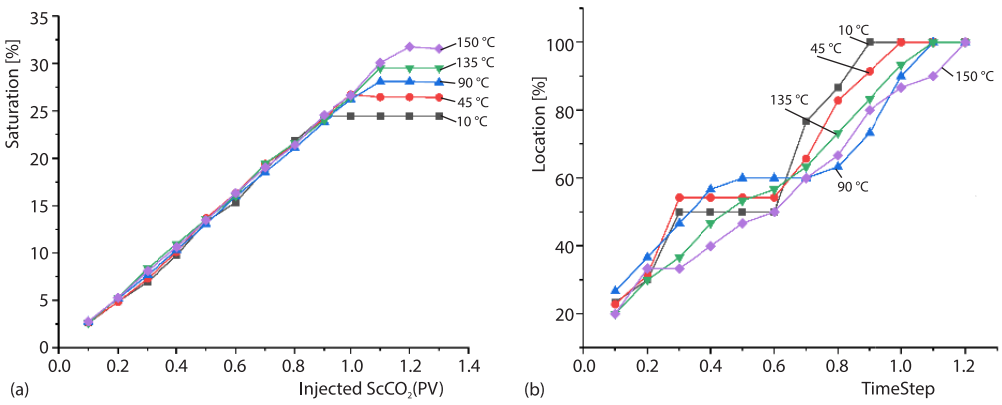

Figure 4. The impact of reservoir wettability on the migration of Sc-CO_2; (a) Sc-CO_2 saturation and (b) normalized frontal distance

Injection speed

In fig. 5, with the increase in injection velocity, CO_2 movement tends to spread in multiple directions rather than a single direction. In fig. 6(a), a higher injection velocity results in a higher final CO_2 saturation and reduces the time to reach the model's outlet. Conversely, a lower

injection velocity leads to a more stepped pattern in the advancement of the Sc-CO_2 front, with more frequent and prolonged pauses, indicating greater flow non-uniformity, as illustrated in fig. 6(b). With increasing injection velocity, the migration speed of Sc-CO_2 gradually accelerates, expanding the reach of the CO_2 plume, increasing total storage, and significantly reducing the project duration.

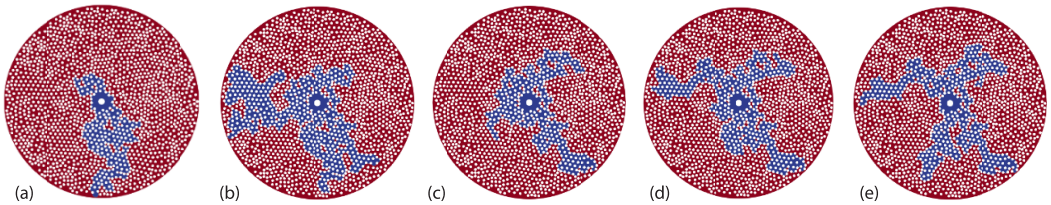

Figure 5. Influence of CO_2 injection velocity on the distribution of Sc-CO_2 fluid; (a) v = 0.0001 m/s, (b) v = 0.0005 m/s, (c) v = 0.0010 m/s, (d) v = 0.0015 m/s, and (e) v = 0.0020 m/s

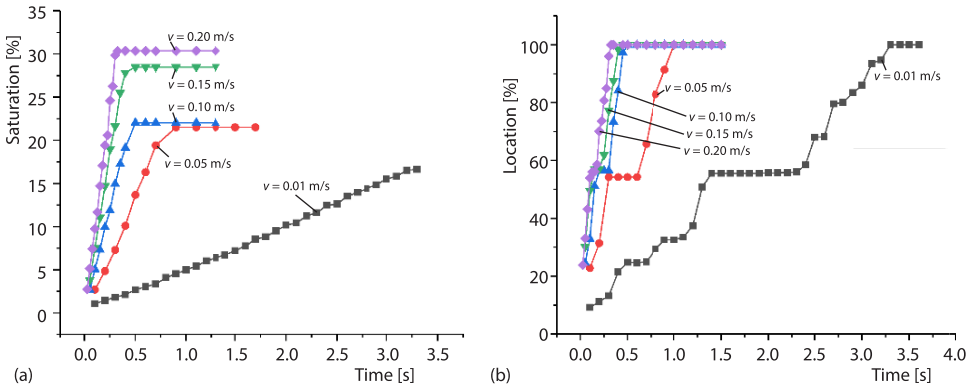

Figure 6. Effect of CO_2 injection velocity on Sc-CO_2 migration; (a) Sc-CO_2 saturation and (b) normalized distance of Sc-CO_2 front

Conclusion

In this study, a simplified reservoir model was established using the fluid volume method to develop a physical and flow model for fluid migration during CO_2 sequestration. The analysis considered various geological and engineering factors affecting CO_2 migration and the secondary distribution of reservoir fluids in actual engineering scenarios. This study, aimed at simplifying computational processes and reducing simulation time, did not account for the chemical changes during the CO_2 storage process or the impact of CO_2 on rock properties. The secondary distribution of reservoir fluids during the CO_2 storage process is a complex phenomenon. Future research should focus on establishing a coupled model integrating heat transfer, fluid-flow, and chemical reactions, considering the comprehensive effects of various factors.

Acknowledgment

This work was supported by Science and Technology Development Project of the Silk Road Economic Belt Innovation Zone, China (No. 2023LQ03005) and Innovation Capability Support of Shaanxi (Program No. 2023-CX-TD-31), Technical Innovation Team for Low Carbon Environmental Protection and Enhanced Oil Recovery in Unconventional Reservoirs.

Nomenclature

$\vec{v}$ – standard specimen edge length, [ms^{-1}]

Greek symbols

ρ – fluid density, [kgm^{-3}]
σ – interfacial tension, [Nm^{-1}]

References

[1] Kai, J., *et al*., The Development of Carbon Capture Utilization and Storage (CCUS) Research in China: A Bibliometric Perspective, *Renewable and Sustainable Energy Reviews*, *138* (2021), 110521
[2] Xie, H., *et al*., Carbon Geological Utilization and Storage in China: Current Status and Perspectives, *Acta Geotechnica*, *9* (2014), 1, pp. 7-27
[3] Xu, Y. Q., *et al*., Numerical Simulation Method and Structural Optimization for Shearing Capacity of Ram Blowout Preventers, *Geoenergy Science and Engineering*, *233* (2024), 212559
[4] Liu, S. Y., *et al*., *The Study on Dispersion Characteristics of Supercritical CO_2-CH_4 Miscible Displacement in Porous Media* (in Chinese), Dalian University of Technology, Dalian, China, 2018
[5] Zhao, G., *et al*., Capillary Sealing Effect and High-pressure Breakthrough Mechanism of Hydrate Reservoir (in Chinese), *Journal of Engineering Thermophysics*, *44* (2023), Mar., pp. 586-591
[6] Oladoyin, K., *et al.*, Impact of Microbial-Rock-CO_2 Interactions on Containment and Storage Security of Supercritical CO_2 in Carbonates, *International Journal of Greenhouse Gas Control*, *120* (2022), 103755
[7] Greenshields, C., Open FOAM User Guide. Version 2.4. 0, Open FOAM Foundation Ltd., 2015
[8] Hu, R., *et al.*, Wettability and Flow Rate Impacts on Immiscible Displacement: A Theoretical Model, *Geophysical Research Letters*, *45* (2018), 7, pp. 3077-3086
[9] Xu, Y. Q., *et al*., Experimental Study on Ultrasonic Wave Propagation Characteristics of Gas-Liquid Two-Phase Flow in Riser Annulus, *Applied Ocean Research*, *141* (2023), 103771
[10] Wang, Y., *et al*., Experimental Study of Crossover from Capillary to Viscous Fingering for Supercritical CO_2-Water Displacement in a Homogeneous Pore Network, *Environ. Sci. Technol*, *47* (2013), 1, pp. 212-218
[11] Xie,P., *et al.*, Micro Model Establishment and Numerical Simulation of Supercritical CO_2 Filtration in Porous Media of Shale Oil Reservoir, *Proceeding*s, 56th U.S. Rock Mechanics/Geomechanics Symposium, Santa Fe, N. Mex., USA, 2022, ID ARMA 22-369
[12] Yang, X. J., The Scaling-Law Flows: An Attempt at Scaling-Law Vector Calculus, *Fractals*, *33* (2024), 4, ID2340126
[13] Yang, X.-J., An Insight on the Fractal Power Law Flow: From a Hausdorff Vector Calculus Perspective, *Fractals*, *30* (2022), 3, ID2250054

Paper submitted: March 20, 2024
Paper revised: March 28, 2024
Paper accepted: May 15, 2024